

Colloidal crystallite suspensions studied by high pressure small angle x-ray scattering

M. A. Schroer, F. Westermeier, F. Lehmkuhler, H. Conrad, A. Schavkan, A. V. Zozulya, B. Fischer, W. Roseker, M. Sprung, C. Gutt, and G. Grübel

Citation: *The Journal of Chemical Physics* **144**, 084903 (2016); doi: 10.1063/1.4941563

View online: <http://dx.doi.org/10.1063/1.4941563>

View Table of Contents: <http://scitation.aip.org/content/aip/journal/jcp/144/8?ver=pdfcov>

Published by the [AIP Publishing](#)

Articles you may be interested in

[Nucleation and crystal growth in a suspension of charged colloidal silica spheres with bi-modal size distribution studied by time-resolved ultra-small-angle X-ray scattering](#)

J. Chem. Phys. **141**, 214906 (2014); 10.1063/1.4902904

[Deformation of diesel soot aggregates as a function of pellet pressure: A study with ultra-small-angle x-ray scattering](#)

J. Appl. Phys. **98**, 073513 (2005); 10.1063/1.2071456

[Grazing-incidence small angle x-ray scattering studies of phase separation in hafnium silicate films](#)

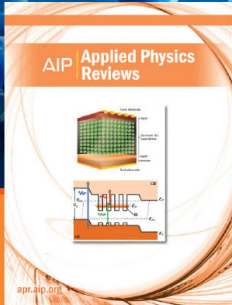
Appl. Phys. Lett. **83**, 3141 (2003); 10.1063/1.1617369

[Pressure-induced structural phase transition of dense droplet microemulsions studied by small-angle x-ray scattering](#)

J. Chem. Phys. **115**, 9496 (2001); 10.1063/1.1413987

[Melting of indium at high pressure determined by monochromatic x-ray diffraction in an externally-heated diamond anvil cell](#)

Appl. Phys. Lett. **78**, 3208 (2001); 10.1063/1.1374497



NEW Special Topic Sections

NOW ONLINE
Lithium Niobate Properties and Applications:
Reviews of Emerging Trends

AIP | Applied Physics
Reviews

Colloidal crystallite suspensions studied by high pressure small angle x-ray scattering

M. A. Schroer,^{1,2,a)} F. Westermeier,³ F. Lehmkuhler,^{1,2} H. Conrad,¹ A. Schavkan,¹
 A. V. Zozulya,¹ B. Fischer,^{1,2,b)} W. Roseker,¹ M. Sprung,¹ C. Gutt,⁴ and G. Grubel^{1,2}

¹Deutsches Elektronen-Synchrotron DESY, Notkestr. 85, 22607 Hamburg, Germany

²The Hamburg Centre for Ultrafast Imaging (CUI), Luruper Chaussee 149,
 22761 Hamburg, Germany

³Max-Planck-Institut für Struktur und Dynamik der Materie, CFEL, Luruper Chaussee 149,
 22761 Hamburg, Germany

⁴Department of Physics, University of Siegen, Walter-Flex-Str. 3, 57072 Siegen, Germany

(Received 4 September 2015; accepted 21 January 2016; published online 25 February 2016)

We report on high pressure small angle x-ray scattering on suspensions of colloidal crystallites in water. The crystallites made out of charge-stabilized poly-acrylate particles exhibit a complex pressure dependence which is based on the specific pressure properties of the suspending medium water. The dominant effect is a compression of the crystallites caused by the compression of the water. In addition, we find indications that also the electrostatic properties of the system, i.e. the particle charge and the dissociation of ions, might play a role for the pressure dependence of the samples. The data further suggest that crystallites in a metastable state induced by shear-induced melting can relax to a similar structural state upon the application of pressure and dilution with water. X-ray cross correlation analysis of the two-dimensional scattering patterns indicates a pressure-dependent increase of the orientational order of the crystallites correlated with growth of these in the suspension. This study underlines the potential of pressure as a very relevant parameter to understand colloidal crystallite systems in aqueous suspension. © 2016 AIP Publishing LLC. [<http://dx.doi.org/10.1063/1.4941563>]

I. INTRODUCTION

Colloidal suspensions serve as model systems to study structure formation processes. Due to the possibility to tailor their properties within the chemical synthesis, colloidal particles of different size, shape, interaction potential, and surface modification can be prepared. Their structural properties are frequently studied by scattering techniques.^{1–5} In particular, large efforts have been undertaken to investigate in detail the effect of external perturbations such as temperature,⁴ electrolyte concentration,^{3,6} shear,^{7,8} electric,^{9,10} and magnetic fields^{11,12} on the phase diagram and phase transitions of concentrated colloidal suspensions. The influence of high hydrostatic pressure on these systems is, however, largely unexplored, mainly due to the involved experimental requirements needed for high pressure studies.

Pressure is one of the fundamental thermodynamic parameters which, in contrast to temperature or chemical potential, affects only the volumetric properties of a sample system. Following Le Chatelier's principle, the application of pressure on a system leads to a reduction of its volume. Pressure-induced changes are, in general, reversible when pressure is released.

Scattering techniques, using hard x-rays or neutrons, offer an excellent possibility to study matter under high pressure due to the high transmission of radiation through the

high absorbing, pressure-sealing windows. These methods are especially powerful to investigate pressure-induced structural changes in soft matter systems. *In situ* scattering studies uncovered the unfolding behavior of proteins in aqueous solutions,^{13–17} phase transitions in lipid and model membrane systems,^{18–20} as well as structural changes in polymers^{21,22} and bio-fibers.^{23,24} The solvent in most of these studies is water as, in particular, all biological-relevant substances are dissolved therein. Water itself has several properties that are susceptible to pressure, such as the change of its density²⁵ and the dielectric constant,²⁶ pressure-induced electrostriction,²⁷ and the change of the pH value.²⁸ Moreover, at pressures close to 2000 bars, the collapse of the second hydration shell in water has been reported, which results in a steep and monotonic increase in the coordination number of water molecules.^{29,30} All these effects give rise to a rich phase behavior of aqueous soft matter samples under high pressure.

For concentrated colloidal suspensions, only a few pressure-assisted studies have been reported so far. These deal mainly with colloids in apolar solvents.^{31–33} To our knowledge, only one study, performed by Okubo in the late 1980s, describes high-pressure effects on charge-stabilized colloidal crystallite suspensions in water.³⁴ In contrast, several small angle scattering studies recently reported on high pressure effects in concentrated aqueous protein solutions.^{35–39} These protein solutions are often modeled as suspensions of small nanoparticles which provides a coarse view of the interactions between the complex macromolecules. In those studies a complex pressure dependence based on the change of the water structure was found.

^{a)}martin.schroer@desy.de

^{b)}Present address: Institut für Physikalische Chemie, University of Hamburg, Grindelallee 117, 20146 Hamburg, Germany

Despite their importance as model systems as well as for possible applications such as photonic crystals,⁴⁰ little is known on the effect of pressure on colloidal crystallites in aqueous suspension. Therefore, we performed high pressure small angle x-ray scattering (SAXS) measurements on aqueous suspensions of charge-stabilized poly-acrylate colloids. We used concentrated suspensions of colloidal crystallites which we expect to be more pressure susceptible than dilute suspensions. Based on the SAXS results a complex interplay between the compression of water with increasing pressure and possible changes of the electrostatic interactions is found. It is this delicate balance between different pressure effects on the solvent and the colloidal crystallites that allows to tune its properties by pressure application. Moreover, it is suggested that for colloidal crystallites, which are in a metastable state due to shear-induced melting within the sample preparation process, the application of pressure and the dilution with water can lead to a similar structural state. In addition, we applied the recently developed x-ray cross correlation analysis (XCCA) to investigate the effect of pressure on the orientational order of the colloidal crystallites. Here, a pressure-induced increase of the orientational order correlated with growth of the crystallites was observed.

The paper is organized as follows. Section II gives an overview of possible effects of high pressure on colloidal suspensions of nanoparticles dispersed in water. Section III describes sample preparation details, the experimental techniques as well as details of data analysis. The following Section IV contains the results and discussion of the SAXS and the XCCA data. The paper ends with a conclusion in Section V.

II. EFFECTS OF HIGH PRESSURE

Applying high pressure forces a sample into the smallest accessible volume. One effect of pressure for aqueous colloidal suspensions is the change of the volume fraction Φ due to the compression of water.²⁵ By increasing pressure, water gets compressed thus reducing the suspension's volume by a factor of $(1 - \kappa_T(p)\Delta p)$, where $\kappa_T(p)$ is the pressure-dependent compressibility of water, and Δp is the pressure difference between pressure p and ambient pressure. This results in an enhanced particle concentration. To describe this pressure-dependent volume fraction $\Phi(p)$ we consider a simple compression model

$$\Phi(p) = \Phi_0 \frac{1}{1 - \kappa_T(p)\Delta p}, \quad (1)$$

wherein Φ_0 is the volume fraction at ambient pressure. This model assumes that the particle volume is not changing with pressure which is valid for our samples and verified in the experiment (see Section IV).

For colloidal crystallites suspended in water and containing water molecules in the unit cell, the compression of water will result in a reduced lattice constant. The relation between the volume fraction of spherical particles of average volume $\langle V_{\text{sph}} \rangle$, i.e., the fraction of space occupied by the particles within the crystal lattice, and the lattice constant in

case of a cubic system with lattice constant a reads

$$\Phi_{\text{cryst}}(p) = N \cdot \frac{\langle V_{\text{sph}} \rangle}{a^3}. \quad (2)$$

Here, N denotes the number of particles within the unit cell. In case of a face-centered cubic (fcc) unit cell one obtains $N = 4$. The index "cryst" indicates that Φ_{cryst} refers to the volume fraction within the crystallites and not to the whole suspension.

For aqueous suspensions, additional effects exist beyond the change of the suspension's density. These pressure effects are based on the electrostatic properties of water and of the charge-stabilized particles. Applying pressure on colloids in water can result in an effective change of the particle interaction strength and thus in a pressure-induced modulation of the particle spacing. The pair interaction potential between charge-stabilized colloidal particles is often well described by a hard sphere repulsion and the repulsive part of the Derjaguin-Landau-Verwey-Overbeek (DLVO) pair potential⁴¹ which reads

$$u_{\text{repuls}}(r) = \frac{e^2}{4\pi\epsilon_0\epsilon_r(p)} \cdot \frac{Z_{\text{eff}}^2(p)}{\left(1 + 0.5\frac{\sigma}{\lambda_D(p)}\right)^2} \cdot \frac{\exp\left(-\frac{r-\sigma}{\lambda_D(p)}\right)}{r}. \quad (3)$$

Here, r denotes the interparticle distance, e the elementary charge, σ the particle diameter, ϵ_0 the vacuum permittivity, and $\epsilon_r(p)$ the pressure-dependent dielectric constant of water. The effective charge $Z_{\text{eff}}(p)$ of the particles can be as well pressure-dependent. The Debye screening length $\lambda_D(p) = \sqrt{(\epsilon_0\epsilon_r(p)k_B T)(e^2 \sum_i n_i z_i^2)^{-1}}$ characterizes the strength of the decay of the electrostatic interaction. T and k_B denote the absolute temperature and Boltzmann's constant, respectively. The screening length depends on the number density n_i of all ion species i and their valence charge z_i (counter-ions, added co-ions as well as the contribution of dissolved and dissociated carbon-dioxide⁴²) and in particular on the pressure. The validity of Eq. (3) and the underlying assumptions involved for the poly-acrylate samples used here was demonstrated by recent SAXS and x-ray photon correlation spectroscopy measurements.⁴³

In order to understand the effects of hydrostatic pressure on charge-stabilized colloids two aspects have to be considered. First, the dielectric constant $\epsilon_r(p)$ of water increases with increasing pressure.²⁶ Following Eq. (3), this change affects the Debye screening length $\lambda_D(p)$ and results in an initially steeper decay of the pair interaction potential with increasing pressure that is similar to an increase of the ion concentration within the solvent.^{31,34} Second, the effective charge $Z_{\text{eff}}(p)$ might increase if the pressure is enhanced resulting in an opposite behavior to the change of the dielectric constant. This effect is based on the fact that water molecules are packed more densely close to charged surfaces.^{44,45} This electrostriction effect leads to an increased local water density and thus reduces effectively the volume.²⁷ A dissociation of counter-ions from the surface of colloids and thus an increase of the effective number of charges can lead to an increased repulsion between the colloidal particles and hence to an increase of the average interparticle distance. Thus in total, in case of crystallites made out of

charge-stabilized colloids, Φ_{cryst} will therefore decrease, whereas the total volume fraction Φ of all colloidal particles within the suspension will increase with increasing compression of water.

Finally, for pressures close to 2000 bars, the molecular structure of the water network starts to change which results in extrema of the diffusion coefficient⁴⁶ and shear viscosity.⁴⁷ More precisely, a steep and monotonic increase of the coordination number was reported resulting in a volume reduction in water, which can be attributed to the penetration of non-hydrogen bonded water molecules into the first coordination shell.^{29,30} This change of the water structure can have an additional effect on the pair interaction potential as was shown for concentrated protein solutions.^{35–39} For these, the interaction potential becomes more attractive close to 2000 bars and above which was assumed to be based on an effective screening of the repulsive interactions due to structural changes of water.

III. MATERIALS AND METHODS

The colloidal samples consisted of charge-stabilized polyacrylate (PA) particles suspended in water. The particles were synthesized by radical emulsion polymerization.⁴⁸ A copolymerization of 1H,1H,5H-octafluoropentylmethacrylate (ABCR GmbH & Co KG, Germany) and methacryloxy-methyltrimethylsilan (ABCR GmbH & Co KG, Germany) was performed at a temperature $T = 60^\circ\text{C}$. To initiate the emulsion polymerization process, $\text{K}_2\text{S}_2\text{O}_8$ (Merck KGaA, Germany) was added, introducing charged sulfate groups. To facilitate the synthesis, a redoxsystem consisting of NaSO_3 (Fluka, Switzerland) and $(\text{NH}_4)_2\text{Fe}(\text{SO}_4)_2$ (Fluka, Switzerland) has been used. Further details of the synthesis can be found in Ref. 43.

Two batches of colloidal particles, called “sample A” and “sample B” in the following, were synthesized with different effective charges ($Z_A = 213 e^-$, $Z_B = 124 e^-$), based on the deprotonation of surface sulfate groups, determined using a particle charge detector (BTG Muetek GmbH), and slightly different particle radii ($\langle R_A \rangle = (86 \pm 1) \text{ nm}$, $\langle R_B \rangle = (79 \pm 1) \text{ nm}$) and particle size polydispersities ($\Delta R_A / \langle R_A \rangle = 4\%$, $\Delta R_B / \langle R_B \rangle = 3\%$) determined by SAXS (see below). The suspensions were concentrated and stored for more than two years in a vessel of 40 ml volume. In this time colloidal crystallites were formed within the whole vessel that can be recognized via the diffraction of visible light resulting in a colored, shiny appearance.

From these two batches pressure-dependent small angle x-ray scattering patterns were recorded. Therefore, a small volume of these suspensions was taken with a pipette from about the upper third part of the stock solution that showed colloidal crystallites, i.e., no sediments from the ground of the vessel were used. These specimens were carefully filled into special sample carriers of 1.8 mm thickness used for the high pressure setup. In addition, a diluted sample was prepared from the stock solution of sample A by diluting four fractions (vol. %) of it with one fraction of deionized water in a test tube. The so prepared suspension was filled as well in a sample holder. When filling the suspension, it is very likely that

part of the crystallites was molten by shear forces. Although samples were used immediately after filling for the SAXS measurements, the time from filling the sample suspension into the SAXS holder to the beginning of the experiment was longer than the time needed for crystallite formation of samples of the given size and surface charge which is several seconds.⁴⁹ Due to this procedure we assume all freshly prepared samples to be homogeneous and to exhibit no sedimentation within the experimental time, i.e., no height dependence present of the sample in the actual sample holder. The resulting volume fractions Φ_{cryst} of the crystals were obtained via Eq. (2) from the lattice constant and gave $\Phi_{\text{cryst}} = 0.17$ for the concentrated aged sample A, $\Phi_{\text{cryst}} = 0.12$ for the diluted sample A, and $\Phi_{\text{cryst}} = 0.07$ for sample B. It has to be noted that besides homogeneous nucleation of the crystallites in the bulk, these can be also formed by heterogeneous nucleation on the polyimide windows as was reported for sample containers of similar dimension than the SAXS sample holder used here.⁴⁹ The formation process of such crystallites is, however, quite complex. Here, we are focussing on the role of pressure in general on colloidal crystallites and do not make any detailed analysis between these two types of crystals.

SAXS experiments were performed at the P10 beamline of PETRA III, DESY, Hamburg.⁵⁰ High pressure conditions were generated using a custom-built high pressure sample cell that employs two flat diamond windows.⁵¹ With this sample cell, a pressure range from 1 bar up to 2600 bars was covered. An x-ray energy of $E = 13 \text{ keV}$ (wavelength $\lambda = 0.0954 \text{ nm}$) was used which results in an x-ray transmission of the sample cell of about 30%. Two-dimensional scattering patterns were recorded by a MAXIPIX detector with a pixel size of $55 \times 55 \mu\text{m}^2$ placed at 5 m distance downstream the sample.⁵² The exposure time per pattern was 0.5 s. The size of the x-ray beam on the sample was $10 \times 10 \mu\text{m}^2$ using beam-defining slits. After a pressure increase, a waiting time of 5 min was applied before the corresponding SAXS patterns were recorded to allow any kinetic changes within the sample to be finished. The sample was moved after each pressure increase to reduce the effect of radiation damage. SAXS measurements were performed at an ambient temperature of $T = 20^\circ\text{C}$. After the SAXS measurements, the sample holders were cleaned with water and dried. Therefore, no measurements on long-time effects after pressurizing the samples could be carried out.

In a SAXS experiment, the scattering intensity $I(\vec{Q})$ is recorded as a function of the wave vector transfer whose modulus is given as $Q = \frac{4\pi}{\lambda} \sin(\Theta/2)$. Herein, λ is the x-ray wavelength and Θ the scattering angle. Using a two-dimensional detector, the scattering patterns are described in terms of Q and the azimuthal angle ϕ , i.e., $I(\vec{Q}) = I(Q, \phi)$. For the SAXS analysis the two-dimensional scattering patterns from the suspensions of colloidal crystallites were corrected for the flatfield and bad pixels of the detector,⁵² azimuthally averaged and the background scattering from the whole sample cell was subtracted. The so-obtained scattering curves

$$I(Q) \propto P_{\text{poly}}(Q) \cdot S(Q) \quad (4)$$

contain the contribution from the polydisperse form factor $P_{\text{poly}}(Q)$ of the PA particles, characterizing their size, shape and polydispersity, and the structure factor $S(Q)$ of the crystal lattice. The form factor contribution was modeled by that from polydisperse spheres using a log-normal distribution function $D_{\text{log-norm}}(R)$ via^{53,54}

$$P_{\text{poly}}(Q) = \frac{\int_0^\infty P_{\text{sph}}(Q, R) \cdot D_{\text{log-norm}}(R) \cdot V_{\text{sph}}^2(R) dR}{\int_0^\infty D_{\text{log-norm}}(R) \cdot V_{\text{sph}}^2(R) dR}. \quad (5)$$

Here, $P_{\text{sph}}(Q, R) = 9[\sin(QR) - QR \cos(QR)]^2 / (QR)^6$ denotes the form factor and $V_{\text{sph}}(R) = 4/3\pi R^3$ the volume of a spherical particle of radius R . The log-normal distribution function gives the best refinement of the experimental data and reads

$$D_{\text{log-norm}}(R) = \frac{1}{\sqrt{2\pi}\sigma R} \exp\left(-\frac{(\ln(R) - \mu)^2}{2\sigma^2}\right), \quad (6)$$

where μ and σ are the parameters describing the shape of the distribution function. These are related to the average particle radius $\langle R \rangle$ and the variance $\text{Var}(R)$ via $\mu = \ln\left(\frac{\langle R \rangle}{\sqrt{\langle R \rangle^2 + \text{Var}(R)}} and $\sigma = \sqrt{\ln\left(1 + \frac{\text{Var}(R)}{\langle R \rangle^2}\right)}$, respectively. The polydispersity is given as $\Delta R / \langle R \rangle = \sqrt{\text{Var}(R) / \langle R \rangle^2}$. The structure factor $S(Q)$ is obtained by dividing the experimental curves by the refined form factors.$

To study the degree of orientational order of the colloidal crystallite suspension as a function of pressure, angular cross correlations from the two-dimensional scattering patterns $I(\vec{Q})$ have been analyzed. The general definition of such an angular cross correlation function of a two-dimensional scattering pattern for fixed Q is given as⁵⁵

$$C(Q, \Delta) = \frac{\langle I(Q, \phi) I(Q, \phi + \Delta) \rangle_\phi - \langle I(Q, \phi) \rangle_\phi^2}{\langle I(Q, \phi) \rangle_\phi^2}, \quad (7)$$

wherein Δ specifies the angle between two radial cross sections through the pattern and $\langle \cdot \rangle_\phi$ denotes the angular average. As was shown in Refs. 55–59, by performing XCCA information on the orientational order within the sample can be obtained. In case of a dominant underlying orientational order, $C(Q, \Delta)$ exhibits characteristic oscillations which can be described by single cosine functions.^{55,56} For a less characteristic shape of $C(Q, \Delta)$, as in case of amorphous systems, the orientational order can be determined by studying the angular Fourier transform of the cross correlation function.^{57–59} For the present case of colloidal crystallite suspensions, the cross correlation function can be well described using the single cosine approach.

IV. RESULTS AND DISCUSSION

A. High pressure SAXS

Figure 1 shows two-dimensional scattering patterns of the concentrated and diluted sample A at two different pressures, respectively.

The concentrated sample A taken from the stock solution exhibits a mainly isotropic scattering pattern at ambient pressure ($p = 1$ bar, Figure 1(a)). Clearly visible is an intense scattering ring at $Q \approx 0.03 \text{ nm}^{-1}$ from strong interparticle correlations. At $Q \approx 0.04 \text{ nm}^{-1}$ six Bragg reflections are present. These are located close to $0^\circ, 60^\circ, 120^\circ, 180^\circ, 240^\circ,$ and 300° (counting clockwise from the positive ordinate). For larger wave vector transfers more isotropic scattering annuli are present that stem from the form factor of the individual particles. The Bragg reflections indicate the presence of oriented crystallites within the suspension at ambient conditions before pressurizing the sample whereas most crystallites seem to be arranged randomly giving rise to the isotropic scattering ring. These findings suggest that this

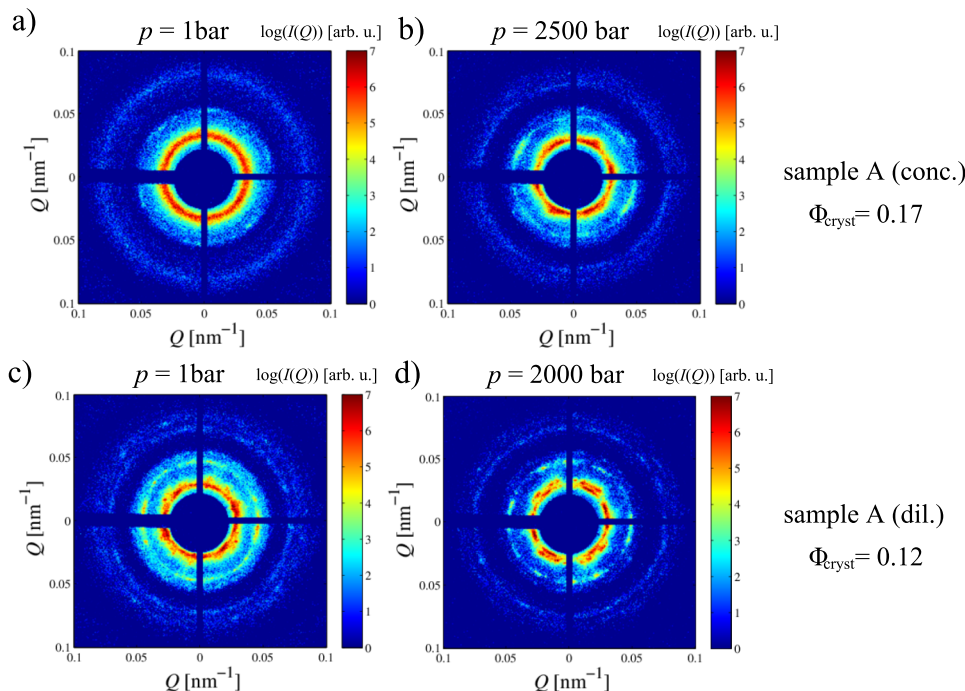


FIG. 1. SAXS patterns for the two types of sample A: concentrated at (a) $p = 1$ bar and (b) $p = 2500$ bars and diluted at (c) $p = 1$ bar and (d) $p = 2000$ bars. Intensity $I(Q)$ is shown on a logarithmic scale. The volume fraction Φ_{cryst} refers to 1 bar. The central part of the patterns is blocked by a beamstop. The stripes between the four quadrants of the MAXIPIX detector indicate zero photon counts and thus appear dark in the image. For the concentrated sample A at 1 bar the scattering pattern is isotropic except for the six Bragg reflections at $Q \approx 0.04 \text{ nm}^{-1}$ separated by 60° with the first reflection between the two top quadrants of the detector. In contrast, at 2500 bars, a clear sixfold symmetry is present. For dilute sample A, several Bragg reflections are visible at both pressures.

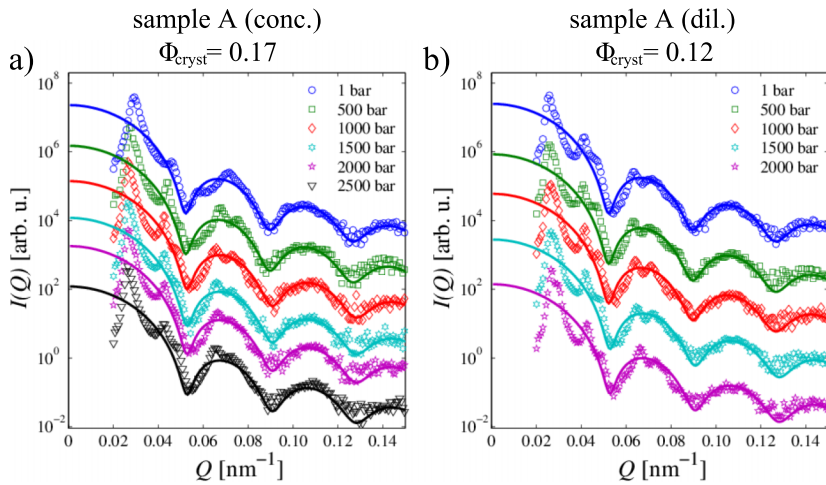


FIG. 2. SAXS intensity $I(Q)$ of two types of sample A for different pressures p : (a) concentrated and (b) diluted. Solid lines are refinements of a form factor of polydisperse spheres. The curves are shifted vertically for clarity.

sample is in a metastable structural state likely due to the shear melting and not fully recrystallization.

Upon increasing the pressure to $p = 2500$ bars (Figure 1(b)), the scattering pattern becomes more textured and exhibits more pronounced Bragg reflections. A clear six-fold symmetry is observed at $Q \approx 0.03 \text{ nm}^{-1}$. This indicates that the crystallites become more oriented with respect to each other when the pressure is increased resulting in effective larger crystallites.

When sample A is diluted to $\Phi_{\text{cryst}} = 0.12$, the SAXS pattern changes and exhibits intense scattering rings with the most prominent one located at $Q \approx 0.025 \text{ nm}^{-1}$ ($p = 1$ bar, Figure 1(c)). This indicates an expansion of the crystalline lattice. The rings are decorated with intense Bragg reflections indicating the presence of oriented crystallites. These might stem from both homogeneous nucleation in the bulk as well as from wall-assisted, heterogeneous nucleation.⁴⁹ Notable, no isotropic ring is present. Increasing the pressure to $p = 2000$ bars (Figure 1(d)), the Bragg reflections become more pronounced. This indicates an increase in the fraction of oriented crystallites in the suspension.

In order to analyze the pressure effect on the crystallite structure in more detail, the azimuthally averaged SAXS curves $I(Q)$ for both types of sample A are shown in Figure 2 for different pressures. The solid lines show the results of a particle form factor fit (see Eq. (5)) modeling the Q -range around the second minimum of the scattering curves from $Q = 0.07$ to 0.12 nm^{-1} which is only weakly affected by modulations of the structure factor $S(Q)$. For small Q the contribution of the structure factor strongly affects the signal, whereas at large Q the scattering intensity is low. The overall scattering signal, however, is of such high quality that the form factor can be extracted directly from the SAXS intensities of the suspensions for all pressures studied. From the fits, an average radius $\langle R \rangle = (86 \pm 1) \text{ nm}$ and a polydispersity of $\Delta R / \langle R \rangle = 4\%$ are obtained for both concentrations of sample A. Both values do not change with pressure, i.e., there is no structural change of the individual nanoparticles on these length scales, as can be also seen from the constant positions of the scattering curves' minima in Fig. 2. For sample B, the average radius is $\langle R \rangle = (79 \pm 1) \text{ nm}$ and $\Delta R / \langle R \rangle = 3\%$. There is no pressure dependence of the particle form factor within

the error bars showing that the particles are not compressible under the studied conditions which is in agreement with the assumption made in Section II.

Looking in more detail at $I(Q)$ one can observe several Bragg reflections below $Q = 0.1 \text{ nm}^{-1}$ (Figure 2). With increasing pressure the position, amplitude, and width of these peaks are changing, pointing to structural changes in the samples. Dividing the scattering curves by the refined form factors allows to access the structure factor $S(Q)$ and thus to study the pressure induced changes more clearly.

Figure 3 depicts the static structure factor $S(Q)$ of both types of sample A for different pressures. We limit our $S(Q)$ analysis here to the Q -range from 0.02 to 0.05 nm^{-1} where three pronounced Bragg reflections are present. The first and third ones both exhibit a shoulder each. For larger Q , peaks are present as well of, however, smaller amplitude. The observed structure factor is best described with that of a face-centered cubic (fcc) phase, which is common for colloidal crystals.^{2,4,34} Here, the first peak and the shoulder arise from the (1,1,1) and (2,0,0) reflections, respectively, the second from the (2,2,0) reflection, and the third one and the corresponding shoulder from the (1,3,1) and (2,2,2) reflections, respectively. Similar reflections are present for sample B. These structure factors are different from that of colloids in the liquid phase⁴³ but are similar to those reported for colloidal particles having been sedimented by centrifugation and crystallized.⁶⁰ It has to be noted that also for the concentrated sample A at ambient pressure showing the most amorphous structure the reflections can be best described by the fcc structure. However, due to the likely metastable state of this sample, additional contributions from similar cubic structures might be present as well.

For the concentrated sample A (Figure 3(a)), a pressure increase from 1 bar to 500 bars leads to an increase of the peak heights. For higher pressures, the peak intensity decreases slightly. There is a change of the peak widths which become more narrow. These pressure induced changes can arise from both changes of the crystallite structure as well as from changes of the crystallite orientation. Determining the average linear crystallite dimension from this width,⁶¹ one finds an increase of it from $\sim 1.8 \mu\text{m}$ to $\sim 3.3 \mu\text{m}$ from 1 bar to 1000 bars. For higher pressures it slightly drops to a value of $\sim 3.0 \mu\text{m}$. For increasing pressure below 1000 bars, the peak

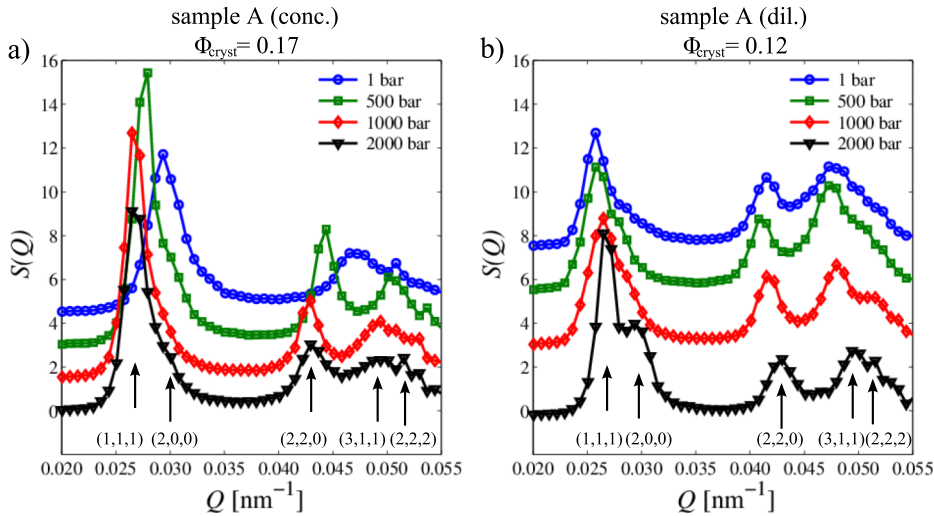


FIG. 3. Structure factor $S(Q)$ for the two types of sample A at different pressures: (a) concentrated and (b) diluted. The positions of the Bragg reflections are indicated by arrows for $S(Q)$ at 2000 bars. Curves were shifted vertically for clarity.

positions shift to smaller Q -values. This would indicate that the lattice constant increases with increasing pressure which differs from the behavior of the other two samples and will be discussed below.

For the diluted sample A (Figure 3(b)), increasing pressure leads to a continuous shift of the Bragg peaks to larger Q . This shows a decrease of the lattice constant a of the crystallite as a function of pressure. The height of the Bragg peaks increases and their width decreases, indicating an increase of the crystallite size from $\sim 2.5 \mu\text{m}$ to $\sim 3.5 \mu\text{m}$. Similar findings hold for sample B.

With increasing pressure the peak positions and thus the lattice constant a of the fcc structure changes as can already be seen in Figure 3. Figure 4 depicts the pressure-dependent lattice constant a for all three samples determined from the peak positions. The positions were obtained by fitting the peaks by Gaussians.

The concentrated sample A has a lattice constant of $a = (394 \pm 6) \text{ nm}$ at ambient pressure. Dilution of the sample with water leads to an increase of it to $a = (440 \pm 8) \text{ nm}$, which indicates that the crystallites' unit cell gets swollen by additional water molecules. Addition of water to the suspension might affect the interparticle interaction between the colloidal particles and thus enhance the interparticle separation as well.

When applying pressure, the lattice constant of these two samples exhibits a different pressure response. For the dilute sample A increasing pressure leads to a decrease of the lattice constant. In order to test whether or not this is caused by the pressure-induced compression of water the simple compression model is used. The solid lines show the pressure-dependent lattice constant employing Eqs. (1) and (2). Within the experimental errors, the data follow this curve. This shows that for the dilute sample A the next neighbor distance inside the colloidal crystallites decreases with increasing pressure when the water density increases.

In contrast, the lattice constant of the concentrated sample A shows a more complex behavior. For pressures up to 1000 bars, a increases and thus does not follow the compression model. For higher pressures, the lattice constant is nearly constant and is similar to that of the diluted sample.

The SAXS data taken for the concentrated sample A under ambient pressure indicate the non-equilibrium, anomalous state of the sample. Instead of strong Bragg peaks a rather isotropic ring of scattering is observed accompanied by a small, compressed lattice constant of $a = (394 \pm 6) \text{ nm}$. Due to potential shear melting of the crystallites by injecting the sample into the SAXS sample holder, possibly a metastable state has been formed which did not happen for the other two samples. This structural states exhibits similarities to those found in crystallized sediments of colloidal particles due to centrifugation.⁶⁰ Addition of water leads to an increase of the lattice constant. A similar effect is present when applying pressure to the concentrated sample. The average crystallite size for both sample A specimens is of similar order and increases with pressure. For pressures close to 1000 bars, the lattice constant for both samples has the same value indicating that a similar final state is reached. This finding resembles the

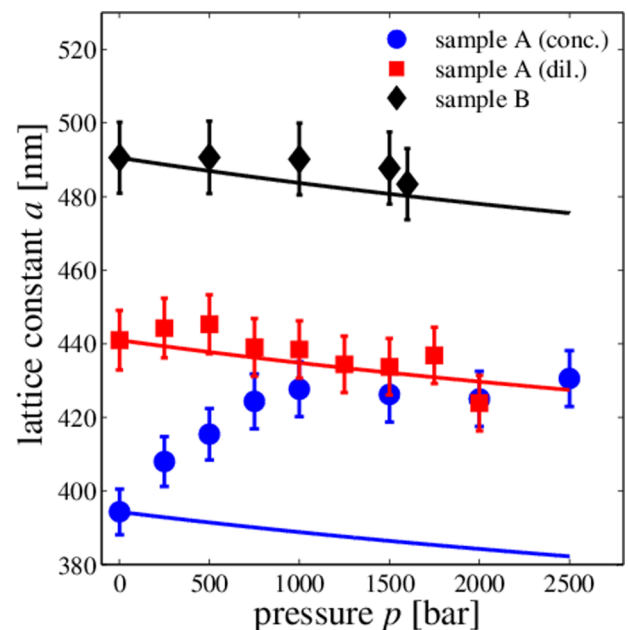


FIG. 4. Lattice constant a as a function of pressure for all samples studied. Solid lines indicate the simple compression model.

expansion of sedimented and crystallized charged particles reported previously.⁶⁰ Our results indicate that application of pressure and dilution of the sample can counter-balance the effects of the shear-induced formation of a metastable state in this sample.

Sample B, which was also stored for more than two years, does show strong Bragg reflections already at ambient pressures indicating the presence of colloidal crystals. We do not observe an anomalous pressure behavior similar to the one of the concentrated sample A as this sample follows the simple compression model. This indicates that subtle changes of the interaction potential and particle concentration can affect the presence of metastable states of colloidal crystallites.

For dilute sample A and sample B the pressure-induced change is reversible. For the concentrated sample A this measurement could not be performed due to limited beamtime.

A possible reason for the anomalous pressure effect in sample A could be the insertion of water molecules into the crystallites unit cell. This might lead to a swelling of the crystallite and an increase of the lattice constant. An increase of the effective particle charge Z_{eff} by deprotonation of surface sulfate groups with pressure up to 1000 bars might take place in addition that may lead to electrostriction of the water molecules in proximity of the particles' surface.²⁷ Such a pressure-induced increase of the particle charge enhances the Coulomb repulsion and thus could lead to larger interparticle separation and consequently a larger lattice constant as well as increase of ordering between the colloidal particles. We note furthermore that the mixing with water changes the effect of pressure on the colloidal crystallites significantly. This points towards a complex dependence on the properties of the solvent. Dilution by the addition of water besides simply swelling the sample may change the dissociation equilibrium of surface sulfate groups such that all of them are already deprotonated. Increasing pressure thus would not change the surface charge but only lead to a compression of the solvent. It is evident that additional theoretical models are needed to confirm this possible mechanism beyond the effect of the pressure-induced compression of water.

It remains to repeat that the pressure-dependence of colloidal crystallites can be well described by the simple compression model. Increasing pressure leads to a decrease of the lattice constant as the water gets compressed. This was demonstrated for the dilute sample A and sample B. Thus, it is possible to fine-tune the lattice spacing of colloidal crystallites by application of pressure in the kbar-range.

B. High pressure XCCA

Information on the pressure dependence of the colloidal crystallites beyond the static structure factor can be obtained by analyzing the angular correlation functions $C(Q, \Delta)$. This is demonstrated for sample A (concentrated) which shows the strongest change of the SAXS patterns. Figure 5 shows $C(Q, \Delta)$ for different pressures from $p = 1$ bar to $p = 2000$ bars. The correlation functions were calculated for Q at the first peak of the structure factor consisting of the (1,1,1) and (2,0,0) reflections.

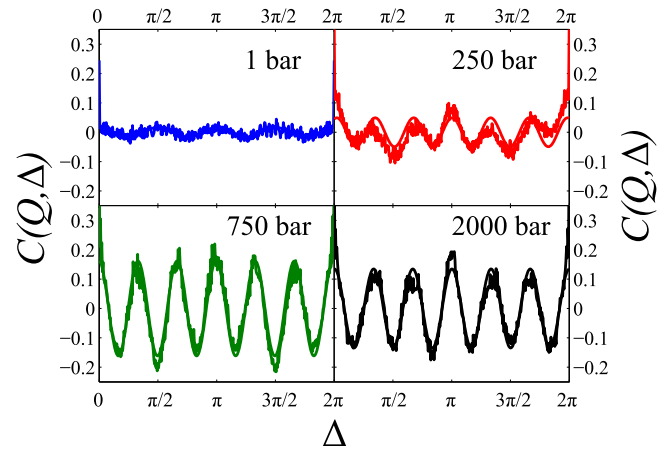


FIG. 5. Angular correlation functions $C(Q, \Delta)$ for sample A (concentrated) at different pressures. $C(Q, \Delta)$ were determined at the vicinity of the first peak of the structure factor $S(Q)$. Fits to $C(Q, \Delta)$ using single cosine functions are shown as well. The cross correlation analysis was performed for $Q = 0.028 \text{ nm}^{-1}$ (1 bar, 250 bars), and $Q = 0.026 \text{ nm}^{-1}$ (750 bars, 2000 bars) with an increment of $\Delta Q = 0.001 \text{ nm}^{-1}$. Different Q had to be chosen as the peak positions shift with pressure.

For $p = 1$ bar, the angular correlation function indicates a weak underlying four-fold orientational order which can be described by a single cosine function. Thus, although the two-dimensional scattering pattern looks isotropic for this Q -value (Figure 1(a)) the cross correlation analysis reveals an underlying weak four-fold order. Note that it has been checked that this four-fold symmetry is not due the quadrant structure of the detector but results from the sample.

Increasing the pressure to $p = 250$ bars, the form of $C(Q, \Delta)$ changes to that of six-fold order. In addition, the amplitude of $C(Q, \Delta)$ increases. Between 250 bars to 750 bars, the amplitude increases even more and the six-fold symmetry becomes more pronounced. For pressures as high as $p = 2000$ bars, the six-fold symmetry persists with similar strength.

The six-fold symmetry at the first maximum for pressures from 250 bars can be understood by the presence of the (1,1,1) reflection. This Bragg reflection refers to lattice planes having six-fold symmetry. The reason for the presence of weak four-fold order at ambient pressure for the first maximum of $S(Q)$ is not so obvious. This sample exhibits a more amorphous structure in comparison to the diluted one. The four-fold order might stem from contributions of (2,0,0) reflection at this Q -value whereas no six-fold order from the (1,1,1) reflections can be seen. However, additional cubic structures might be present which could give a similar weak signal. This weak four-fold order thus again supports the finding that this sample has been in a metastable state before pressure was applied. Note that for the (2,2,2) reflection a six-fold symmetry can be found which underlines again the dominance of the fcc structure ((Fig. 1(a)), XCCA data not shown). As the amplitude of the angular correlation functions $C(Q, \Delta)$ is small at 1 bar, the colloidal crystallites are eventually more randomly distributed within the suspension. This changes with increasing pressure, as the six-fold symmetry of the scattering patterns increases. For the other reflections, the XCCA signal is in general weaker but also shows an increase of orientational order with pressure (data not shown). This

reflects a higher preferred orientational order between the crystallites, i.e., these show a non-random orientational order. Thus, the XCCA data suggest a pressure induced effect similar to an increase of crystallite alignment starting from 250 bars and continuing up to 750 bars and thus accompanying the sample changes into a different structural state. For higher pressures, the orientational order does not change any more.

The observed orientational order for concentrated sample A exhibits a similar pressure dependence as the previously discussed lattice constant and of the average crystallite size, i.e., a pronounced change within a pressure range from 1 to 750 — 1000 bars and only a weak change for higher pressures. The sample that was in a less-ordered state before becomes more ordered by application of pressure. This hints to a common pressure-dependent mechanism that affects both the interparticle interaction and the orientational order between different crystallites. This possibly leads to a slightly pressure-induced growth of crystallites favoring orientational order. Overall, the findings indicate a pressure-induced change of the crystallite structure from a metastable to a stable state.

V. CONCLUSION

The effect of high hydrostatic pressure on colloidal crystallite suspensions made from poly-acrylate particles was studied for the first time by SAXS. As these charge-stabilized particles are suspended in water, a complex pressure dependence of the crystalline properties and the orientational order within these samples is observed. This was shown for the fcc structure based on the changes of the structure factor peak and the lattice constant as pressure was applied and points to a delicate interplay between water compression, swelling, and changes of the electrostatic properties of the colloidal crystallites.

For the dilute sample A and sample B the water compression seems to be the dominant mechanism as the results can be explained very well in terms of the simple compression model introduced. Increasing pressure thus reduces the crystallites' lattice constant and allows to tune their properties. In contrast, the most concentrated sample (concentrated sample A) deviates from this simple model and shows for pressure up to $p = 1000$ bars the opposite effect indicating the presence of a metastable state. For this particular sample being most likely in a metastable state induced by shear-induced melting, the addition of water and the application of pressure seem to result in a similar final structural state. These structural changes are similar to the expansion and crystallization of charged colloidal spheres.⁶⁰ Future studies might focus on colloidal samples sedimented by gentle centrifugation to avoid the long-time storage.

As discovered by the XCCA technique, application of pressure can increase the orientational order between the colloidal crystallites. This was demonstrated for the concentrated sample A which showed that XCCA is more sensitive to structural changes than the conventional SAXS analysis. The observed increase of the preferential ordering from a mostly random configuration sets in the same pressure range as the pressure-induced expansion of the lattice constant and crystallite growth hinting to a common mechanism.

One possible explanation for the anomalous findings of the concentrated sample A that is likely to have been in a metastable state is a pressure-induced swelling and a change of the effective particle charge resulting in an increased lattice constant. As was pointed out, changes of the ionic properties might be favored by pressure differences. Similar mixing sample A with water might induce changes in the suspension's ionic properties. The pressure response for the concentrated sample at $p = 1000$ bars could be understood by an increase of the effective particle charge with pressure due to electrostriction of water up to 1000 bars. For higher pressures, all ionizable groups on the particle surface might be ionized and, thus, a further increase of pressure will not change it, leaving the compression of water the dominant contribution. In addition to these effects, the changes of the molecular water structure setting in at 2000 bars might affect the colloidal crystallite suspension as well. For a complex pressure mechanism based on the systems' electrostatic properties more elaborate models are needed.

Our study shows that high pressure has a complex influence on charge stabilized colloidal systems that depends on the solution's properties. The most dominant effect is the pressure-induced decrease of the lattice constant that is due to the compression of the solvent. Based on this finding, it should be possible to fine-tune the crystallite structure by pressure and the suspension's characteristics. These manipulations might be of relevance for applications in photonic crystals based on colloidal crystals. As the wavelength acceptance of these depends on the lattice constant,^{62,63} pressure application might be a tool to manipulate it in a desired way. Contrary, the wavelength acceptance of these crystals might be used for pressure detection and thus colloidal crystals might be employed as pressure sensors.

ACKNOWLEDGMENTS

The authors thank R. Winter and M. Tolan for sharing the high pressure equipment and J. Möller for shipping. This work has been supported by the excellence cluster "The Hamburg Centre for Ultrafast Imaging — Structure, Dynamics, and Control of Matter at the Atomic Scale" of the DFG. H.C. acknowledges financial support by the Deutsche Forschungsgemeinschaft within the framework of the graduate school 1355 "Physics with new advanced coherent radiation sources." Parts of this research were carried out at beamline P10 at the light source PETRA III at DESY, a member of the Helmholtz Association (HGF).

¹P. N. Pusey and W. Van Meegen, *Nature* **320**, 340 (1986).

²E. B. Sirota, H. D. Ouyang, S. K. Sinha, P. M. Chaikin, J. D. Axe, and Y. Fujii, *Phys. Rev. Lett.* **62**, 1524 (1989).

³A. Mourchid, A. Delville, J. Lambard, E. Lecolier, and P. Levitz, *Langmuir* **11**, 1942 (1995).

⁴U. Gasser, J. J. Liator-Santos, A. Scotti, O. Bunk, A. Menzel, and A. Fernandez-Nieves, *Phys. Rev. E* **88**, 052308 (2013).

⁵T. Palberg, *J. Phys.: Condens. Matter* **26**, 333101 (2014).

⁶E. Dubois, R. Perzynski, F. Boue, and V. Cabuil, *Langmuir* **16**, 5617 (2000).

⁷B. J. Ackerson and N. A. Clark, *Physica A* **118**, 221 (1983).

⁸H. Löwen, *J. Phys.: Condens. Matter* **13**, R415 (2001).

⁹P. S. Mohanty, A. Yethiraj, and P. Schurtenberger, *Soft Matter* **8**, 10819 (2012).

- ¹⁰B. Liu, T. H. Besseling, M. Hermes, A. F. Demirors, A. Imhof, and A. van Blaaderen, *Nat. Commun.* **5**, 3092 (2014).
- ¹¹J. Wagner, B. Fischer, and T. Autenrieth, *J. Chem. Phys.* **124**, 114901 (2006).
- ¹²A. B. G. M. Leferink Op Reinink, S. Belli, R. van Rooij, M. Dijkstra, A. V. Petukhov, and G. J. Vroege, *Soft Matter* **10**, 446 (2014).
- ¹³V. K. Aswal, S. Chodankar, J. Kohlbrecher, R. Vavrin, and A. G. Wagh, *Phys. Rev. E* **80**, 011924 (2009).
- ¹⁴J. B. Rouget, M. A. Schroer, C. Jeworrek, M. Puehse, J. L. Saldana, Y. Bessin, M. Tolan, D. Barrick, R. Winter, and C. A. Royer, *Biophys. J.* **98**, 2712 (2010).
- ¹⁵M. A. Schroer, M. Paulus, C. Jeworrek, C. Krywka, S. Schmacke, Y. Zhai, D. C. F. Wieland, C. J. Sahle, M. Chimenti, C. A. Royer, B. Garcia-Moreno, M. Tolan, and R. Winter, *Biophys. J.* **99**, 3430 (2010).
- ¹⁶R. Kitahara, K. Hata, A. Maeno, K. Akasaka, M. S. Chimenti, B. Garcia-Moreno, M. A. Schroer, C. Jeworrek, M. Tolan, R. Winter, J. Roche, C. Roumestand, K. Montet de Guillen, and C. A. Royer, *Proteins: Struct., Funct., Bioinf.* **79**, 1293 (2011).
- ¹⁷G. Gibrat, G. H. B. Hoa, C. T. Craescu, L. Assairi, Y. Blouquit, B. Annighoefer, R. P. May, and M. C. Bellissent-Funel, *Biochim. Biophys. Acta* **1844**, 1560 (2014).
- ¹⁸R. Winter and C. Jeworrek, *Soft Matter* **5**, 3157 (2009).
- ¹⁹N. J. Brooks, O. Ces, R. H. Templer, and J. M. Seddon, *Chem. Phys. Lipids* **164**, 89 (2011).
- ²⁰N. J. Brooks, *IUCr* **1**, 470 (2014).
- ²¹J. J. Litor-Santos, U. Gasser, R. Vavrin, Z. B. Hu, and A. Fernandez-Nieves, *J. Chem. Phys.* **133**, 034901 (2010).
- ²²S. Grobelny, C. H. Hofmann, M. Erlkamp, F. A. Plamper, W. Richtering, and R. Winter, *Soft Matter* **9**, 5862 (2013).
- ²³R. Ene, C. Krywka, S. G. Kang, P. Papadopoulos, M. Burghammer, E. Di Cola, M. Müller, and F. Kremer, *Polymer* **53**, 5507 (2012).
- ²⁴C. Krywka, I. Krasnov, R. Figuli, M. Burghammer, and M. Müller, *Macromolecules* **47**, 7187 (2014).
- ²⁵R. A. Fine and F. J. Millero, *J. Chem. Phys.* **59**, 5529 (1973).
- ²⁶W. B. Floriano and M. A. C. Nascimento, *Braz. J. Phys.* **34**, 38 (2004).
- ²⁷I. Danielewicz-Ferchmin, E. M. Banachowicz, and A. R. Ferchmin, *Phys. Chem. Chem. Phys.* **13**, 17722 (2011).
- ²⁸R. C. Neuman, W. Kauzmann, and A. Zipp, *J. Phys. Chem.* **77**, 2687 (1973).
- ²⁹A. K. Soper and M. A. Ricci, *Phys. Rev. Lett.* **84**, 2881 (2000).
- ³⁰G. Weck, J. Eggert, P. Loubeyre, N. Desbiens, E. Bourasseau, J. B. Maillet, M. Mezouar, and M. Hanfland, *Phys. Rev. B* **80**, 180202 (2009).
- ³¹C. G. De Kruif and J. A. Schouten, *J. Chem. Phys.* **92**, 6098 (1990).
- ³²G. Meier, R. Vavrin, J. Kohlbrecher, J. Buitenhuis, M. P. Lettinga, and M. Ratajczyk, *Meas. Sci. Technol.* **19**, 034017 (2008).
- ³³R. Vavrin, J. Kohlbrecher, A. Wilk, M. Ratajczyk, M. P. Lettinga, J. Buitenhuis, and G. Meier, *J. Chem. Phys.* **130**, 154903 (2009).
- ³⁴T. Okubo, *J. Chem. Soc., Faraday Trans. 1* **84**, 1949 (1988).
- ³⁵M. A. Schroer, J. Markgraf, D. C. F. Wieland, C. J. Sahle, J. Moeller, M. Paulus, M. Tolan, and R. Winter, *Phys. Rev. Lett.* **106**, 178102 (2011).
- ³⁶M. A. Schroer, Y. Zhai, D. C. F. Wieland, C. J. Sahle, J. Nase, M. Paulus, M. Tolan, and R. Winter, *Angew. Chem., Int. Ed.* **50**, 11413 (2011).
- ³⁷M. A. Schroer, M. Tolan, and R. Winter, *Phys. Chem. Chem. Phys.* **14**, 9486 (2012).
- ³⁸J. Möller, M. A. Schroer, M. Erlkamp, S. Grobelny, M. Paulus, S. Tiemeyer, F. J. Wirkert, M. Tolan, and R. Winter, *Biophys. J.* **102**, 2641 (2012).
- ³⁹J. Möller, S. Grobelny, J. Schulze, S. Bieder, A. Steffen, M. Erlkamp, M. Paulus, M. Tolan, and R. Winter, *Phys. Rev. Lett.* **112**, 028101 (2014).
- ⁴⁰A. Blanco, E. Chomski, S. Grachtak, M. Ibisate, S. John, S. W. Leonard, C. Lopez, F. Meseguer, H. Miguez, J. P. Mondia, G. A. Ozin, O. Toader, and H. M. van Driel, *Nature* **405**, 437 (2000).
- ⁴¹E. J. W. Verwey and J. T. G. Overbeek, *Theory of the Stability of Lyophobic Colloids* (Elsevier, New York, 1948).
- ⁴²F. J. Millero, *Geochim. Cosmochim. Acta* **59**, 661 (1995).
- ⁴³F. Westermeier, B. Fischer, W. Roseker, G. Grübel, G. Nägele, and M. Heinen, *J. Chem. Phys.* **137**, 114504 (2012).
- ⁴⁴M. F. Toney, J. N. Howard, J. Richer, G. L. Borges, J. G. Gordon, O. Melroy, D. Wiesler, D. Yee, and L. Sorensen, *Nature* **368**, 444 (1994).
- ⁴⁵D. I. Svergun, S. Richard, M. H. J. Koch, Z. Sayers, S. Kuprin, and G. Zaccai, *Proc. Natl. Acad. Sci. U. S. A.* **95**, 2267 (1998).
- ⁴⁶R. Ludwig, *Angew. Chem., Int. Ed.* **40**, 1808 (2001).
- ⁴⁷P. G. Debenedetti, *J. Phys.: Condens. Matter* **15**, R1669 (2003).
- ⁴⁸S. C. Thickett and R. G. Gilbert, *Polymer* **48**, 6965 (2007).
- ⁴⁹P. Wette, A. Engelbrecht, R. Salh, I. Klassen, D. Menke, D. M. Herlach, S. V. Roth, and H. J. Schoepe, *J. Phys.: Condens. Matter* **21**, 464115 (2009).
- ⁵⁰A. V. Zozulya, S. Bondarenko, A. Schavkan, F. Westermeier, G. Grübel, and M. Sprung, *Opt. Express* **20**, 18967 (2012).
- ⁵¹C. Krywka, C. Sternemann, M. Paulus, M. Tolan, C. Royer, and R. Winter, *ChemPhysChem* **9**, 2809 (2008).
- ⁵²A. Schavkan, F. Westermeier, A. Zozulya, A. Bondarenko, G. Grübel, C. Schroer, and M. Sprung, *J. Phys.: Conf. Ser.* **425**, 202004 (2013).
- ⁵³*Neutron, X-rays and Light. Scattering Methods Applied to Soft Condensed Matter*, edited by P. Linder and T. Zemb (North Holland, 2002).
- ⁵⁴G. Beaucage, H. K. Kammler, and S. E. Pratsinis, *J. Appl. Cryst.* **37**, 523 (2004).
- ⁵⁵P. Wochner, C. Gutt, T. Autenrieth, T. Demmer, V. Bugaev, A. Diaz Ortiz, A. Duri, F. Zontone, G. Grübel, and H. Dosch, *Proc. Natl. Acad. Sci. U. S. A.* **106**, 11511 (2009).
- ⁵⁶C. Gutt, L. Grodd, E. Mikayelyan, U. Pietsch, J. Kline, and S. Grigorian, *J. Phys. Chem. Lett.* **5**, 2335 (2014).
- ⁵⁷F. Lehmkuhler, G. Grübel, and C. Gutt, *J. Appl. Cryst.* **47**, 1315 (2014).
- ⁵⁸M. A. Schroer, C. Gutt, and G. Grübel, *Phys. Rev. E* **90**, 012309 (2014).
- ⁵⁹M. A. Schroer, C. Gutt, F. Lehmkuhler, B. Fischer, I. Steinke, F. Westermeier, M. Sprung, and G. Grübel, *Soft Matter* **11**, 5465 (2015).
- ⁶⁰J. S. van Duijneveldt, J. K. G. Dhont, and H. N. W. Lekkerkerker, *J. Chem. Phys.* **99**, 6941 (1993).
- ⁶¹J. I. Langford and A. J. C. Wilson, *J. Appl. Cryst.* **11**, 102 (1978).
- ⁶²J. D. Joannopoulos, P. R. Villeneuve, and S. H. Fan, *Nature* **386**, 143 (1997).
- ⁶³K. Lee and S. A. Asher, *J. Am. Chem. Soc.* **122**, 9534 (2000).